Received: 18 November 2020 | Revised: 3 February 2021 | Accepted: 2 March 2021

IET Generation, Transmission & Distribution

DOI: 10.1049/gtd2.12169

The Institution of Engineering and Technology WILEY

ORIGINAL RESEARCH PAPER

Analysis of instability causes in the bi-dc converter and enhancing its performance by improving the damping in the IDA-PBC control

Gang Lin[1] | Jiayan Liu[1] | Christian Rehtanz[1] | Yong Li[2] | Wei Zuo[3] | Pengcheng Wang[4]

[1] Institute of Energy Systems, Energy Efficiency and Energy Economics (ie3), TU Dortmund University, Dortmund, Germany

[2] The College of Electrical and Information Engineering, Hunan University, Changsha, China

[3] The College of Electrical Engineering, University of Leeds, Leeds, UK

[4] The College of Electrical Engineering, Zhejiang University, Hangzhou, China

Correspondence
Gang Lin, ie3, TU Dortmund University, Dortmund 44227, Germany.
Email: 1287937851@qq.com

Funding information
China Scholarship Council, Grant/Award Number: 201906130196

Abstract

The poor damping of bidirectional dc (bi-dc) converter caused by constant power load makes power system prone to oscillation, and non-minimum phase characteristic also jeopardises voltage stability. To solve these challenges, the interconnection and damping assignment passivity-based control (IDA-PBC) is utilised to improve transient response. The influences of the right-half-plane (RHP) zero on the stability margin and controller design are illustrated by zero dynamics analysis. Then the port-controlled Hamiltonian modelling is used to obtain the IDA-PBC control law, which is suitable to the bi-dc converter and independent of the operation mode. The system dissipation property is modified, and thus the desired damping is injected to smooth the transient voltage. To remove the voltage error caused by RHP zero and adjust the damping ratio, an energy controller with an adjustment factor is introduced. Besides, a virtual circuit is established to explain the physical meaning of the control parameter, and the parameter design method is given. Passivity analysis assesses the controller performance. Simulation results are analysed and compared with other control strategies to test the proposed IDA-PBC strategy.

1 | INTRODUCTION

In recent years, the dc system has become the potential alternative to the ac system in some scenarios and is widely used in the field of shipboards, electric vehicles and smart buildings [1–4]. A typical topology of a single bus dc distribution network is shown in Figure 1, consisting of photovoltaic (PV) generation, an energy storage system (ESS) including battery, and ac/dc loads. This dc distribution network is connected to the utility grid and/or ac microgrid (ac-MG) via a grid-connecting converter. The load converters are generally controlled by a high bandwidth regulator. Therefore, constant power loads (CPLs) occur, destructing the stability and even making the system unstable [5–10]. Besides, some special converters, such as bidirectional dc (bi-dc) converter, is influenced by CPLs and right-half-plane (RHP) zero. RHP zero makes the system non-minimum phase characteristics, degrading the stability margin and making the controller design difficult. Therefore, advanced control methods need to be developed to improve the system damping and maintain robust voltage regulation against the influence of RHP zero.

The stability challenges of dc converters can be solved by either passive damping [6] or active damping [7, 8] methods. Adding a passive damper can effectively address the stability problem [6], but the system complexity will inevitably be increased and the system efficiency is reduced. In the active damping methods, the virtual impedance method is adopted in [7, 9] to reshape the output impedance of voltage regulation converters and the input impedance of load converters in dc MG, respectively. However, the load performance might be influenced. To fulfil the impedance-based stability criterion, the output impedance of converters is modified to stabilise the system [10]. An inertia emulation approach is proposed in [11] to control the external characteristics of converters and improve their dynamic response. From the perspective of passivity theory, system passivity can be enforced through the controlled

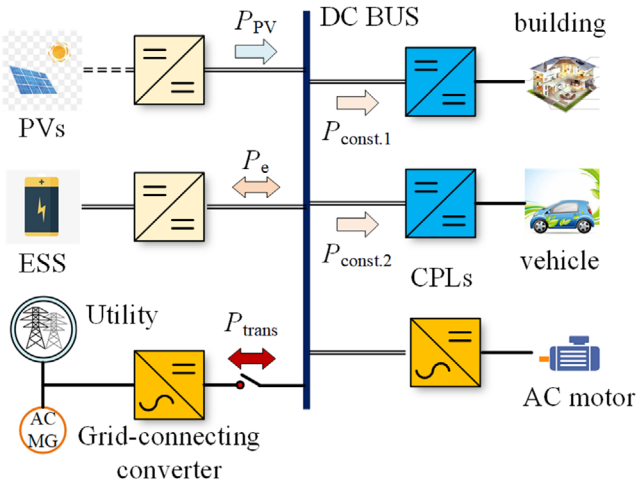

FIGURE 1 Typical topology of single bus dc distribution network

active damping impedances [12]. The dc voltage is indirectly stabilised by passivity-based control (PBC) with the Brayton–Moser framework, and the series or parallel damping based solutions are used to solve the issue of the error dynamic [13]. A simplified parallel-damped passivity-based controller is proposed in [14] to maintain its robust output voltage regulation and a complementary proportional integral derivative (PID) controller is designed to remove the steady-state error. The classical linear controllers are simple to design and implement, but there are difficulties in dealing with the uncertainty of system parameters, and the RHP zero is ignored.

The PBC, one kind of non-linear control method, could achieve energy shaping by a damping injection matrix, and its control law is easily implemented using the structure property of the physical system [28]. The virtual damping injection is realised and the voltage regulation issue is addressed [19]. The port-controlled Hamiltonian (PCH) model describes the energy interaction via ports between the modelled system and the external environment. Interconnection and damping assignment-PBC (IDA-PBC) can achieve the active damping control of PCH systems by modifying the energy interchange and dissipation, and the transient response is improved [16, 17]. It is worth noting that the arbitrary interconnection system of IDA-PBC will maintain stable because the passivity is preserved in the resulting systems [27].

Based on the passivity theory, [15] proposes a non-linear controller to change the system energy dissipation property and enhance the voltage regulation ability against system parameters variation. The voltage stability challenge of the dc MG is addressed in [27] by applying the IDA-PBC method to the PCH model of source-side converters. In [18], IDA–PBC technique is utilised in the voltage outer loop and the damping performance is improved. In addition, an extra integral loop is used to eliminate the voltage error. The PCH model of power electronic transformer is built in [19], and IDA-PBC is applied to address its voltage regulation issue. Adaptive IDA-PBC can also be used to solve the issue that bi-dc converter is non-minimum phase characteristic [20]. But the model only considers the buck state. In [21], an improved IDA-PBC scheme is proposed to make the interconnection matrix adaptive. The PCH models for dc converter is established, and the unique control equations are acquired. The IDA-PBC is utilised in [22] to ensure cascaded system stability via using the Hamiltonian function, and the dynamics instability issue is solved. In [23], the boost converter is modelled as a PCH system, and the damping performance is improved by an adaptive IDA-PBC method. Besides, an equivalent circuit is derived and control parameters are determined. In [24], a modified IDA-PBC is proposed to ensure the passivity property of *LC* input filter-dc/dc converter system, considering the interaction between *LC* filter and converters. Combined with the modified IDA-PBC, a non-linear observer is presented in [25] to eliminate the steady-state errors and reduce the number of sensors. In [26], an adaptive energy shaping control based on the IDA-PBC is developed to ensure the large-signal stability of the power converter with an input filter.

The above works do not study the application of IDA-PBC in bi-dc converter whose instability cause is related to its operation state, and the influence of its RHP zeros on the controller design is ignored. Because of the poor damping of the bi-dc converter supplying CPLs, it is necessary to study an IDA-PBC control law that is suitable for both boost and buck states. Meanwhile, the zero dynamics is studied to guide the controller design and better control performance can be acquired.

In this paper, the zero dynamics of bi-dc converter in both boost and buck state is analysed to elaborate its instability causes and its constraint on controller design. The IDA-PBC control law is derived for bi-dc converter via modifying the energy interchange and dissipation property. Based on the results of zero dynamics analysis, the reasonable IDA-PBC control law is selected to make the system passivity, and a proportional integral (PI) controller with an adjustment factor k is added to regulate the steady-state response. A virtual circuit is established to design parameters, and the reasonable range of r_1 and k could be determined by eigenvalue analysis. Passivity analysis is given to verify the proposed method.

The contributions of this paper are:

1. From the perspective of the RHP zero dynamics, the instability causes of the bi-dc converter is illustrated. The constraints on the controller design are studied, which can be used to guide the IDA-PBC design.
2. PBC method, which is suitable for bi-dc converter and independent of its operation mode, is proposed. IDA-PBC forms the current inner loop, which modifies the energy dissipation and increases system damping, to improve transient response. The outer loop consists of an energy controller with an adjustment factor k, reducing the voltage error.
3. A virtual circuit is established to explain the physical significance of the control parameter. The range of parameters are determined via eigenvalue analysis, and passivity analysis verifies the effect of the proposed method.

The rest of the paper is given as follows. The studied topology introduction and RHP zero dynamics analysis are in Section 2. The IDA-PBC control law is obtained and the energy regulator is designed in Section 3. The virtual circuit is established in

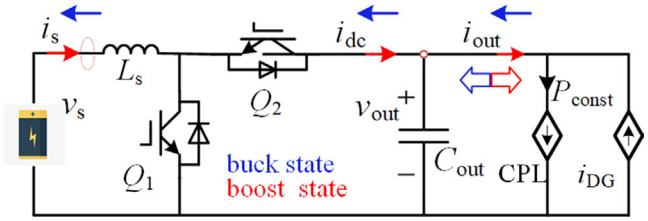

FIGURE 2 The simplified circuit of single bus dc distribution network

Section 4. The dynamic and passivity analyses are in Section 5. Section 6 verifies the proposed control method by simulation, and Section 7 gives the conclusion.

2 | MODEL AND PROBLEM DESCRIPTION

This article focuses on designing the passive controller for ESS converters in parallel operation and stabilising the bus voltage of dc distribution network. Therefore, with the introduced virtual resistance, the converter is enforced passivity and the damping improvement is achieved.

The ESS is connected to the dc bus through the buck-boost converter (the bi-dc converter studied in this article) and the voltage transformation is achieved. The simplified circuit of Figure 1 is depicted in Figure 2. By controlling Q_1, the boost operation (red arrow) is achieved, and the buck operation (blue arrow) is realised by controlling Q_2; the trigger pulses are complementary, namely, $d_{1\_buck} = 1\text{-}d_{1\_boost}$. d_{1_buck} and d_{1_boost} are the duty ratio in buck and boost state, respectively. L_s and C_{out} are the input filter inductance and output capacitor, v_s is the output voltage of ESS and i_s is the inductance current. v_{out} is the voltage across the output capacitor, and i_{out} is the output current through the line. PV and CPLs can be equivalent to a current source. P_{const} is the consuming power of CPLs and i_{PV} is the equivalent output current of PV. Zero dynamics of bi-dc converter is investigated in this section.

2.1 | Modelling and zero dynamics analysis in boost state

When the bi-dc converter operates forward (i.e. boost state), its state-space equation is shown in Equation (1).

$$\begin{cases} L_s \dfrac{di_s}{dt} = v_s - uv_{out} \\ C_{out} \dfrac{dv_{out}}{dt} = ui_s - \dfrac{P_{const}}{v_{out}} \end{cases} \tag{1}$$

where $u = 1-d_{1\_boost}$ is the input signal. For the system in Equation (1), the set of the equilibrium point is ε_{x1} as shown in Equation (2).

$$\varepsilon_{x1} = \left\{ (i_s, v_{out}) \in R^2_{>0} \middle| v_s i_s - P_{const} = 0 \right\} \tag{2}$$

When the bi-dc converter operates in the boost state, the following two *conclusions* could be obtained. The subscript '*' stands for steady-state value.

1. Corresponding to the output $y_1 = v_{out} - v_{out*}$, the zero dynamics characteristic is unstable.
2. Corresponding to the output $y_2 = i_s - i_{s*}$, the zero dynamics characteristic is stable, but it is not attractive at v_{out*}.

Proof: Based on the second formula in Equation (1), $u = P_{const}/(i_s \bullet v_{out*})$ can be derived when $v_{out} = v_{out*}$. Accordingly, Equation (3) can be obtained by combining this result and the first equation in Equation (1).

$$\frac{di_s}{dt} = \frac{v_s}{L_s} - \frac{P_{const}}{L_s i_s} := f_1(i_s) \tag{3}$$

The slope of $f_1(i_s)$, when $i_s = i_{s*}$, is expressed as

$$\left(f_1(i_s)\big|_{i_s = i_{s*}} = \frac{P_{const}}{L_s i_{s*}^2} > 0 \right. \tag{4}$$

Hence, it is proved that the system in Equation (1) at i_{s*} is unstable.

On the other hand, based on the first formula in Equation (1), $u = v_s/v_{out}$ can be derived when $i_s = i_{s*}$. Accordingly, Equation (5) can be obtained by combining this result and the second equation in Equation (1).

$$\frac{dv_{out}}{dt} = \frac{1}{C_{out} v_{out}} (v_s i_{s*} - P_{const}) \equiv 0 \tag{5}$$

Hence, it is proved that the system in Equation (1) is stable at the equilibrium point v_{out*}, but it is not attractive.

Remark 1: The bi-dc converter, regarded as the boost circuit, is prone to make the system unstable because of non-minimum phase characteristics. The influence of CPLs exacerbates this instability as stated in Equations (4) and (5).

Remark 2: From the analysis mentioned above, the zero dynamics characteristic, corresponding to i_s, is stable, but it is not attractive at v_{out*}. Therefore, a steady-state voltage error would be caused depending on the initial condition, when a regulator is designed to control i_s then indirectly controlling v_{out}.

Remark 3: Designing a controller becomes difficult. The RHP zero limits the system bandwidth, making the dynamic response significantly slow.

2.2 | Modelling and zero dynamics analysis in buck state

When the bi-dc converter operates in reverse (i.e. buck state), the state-space equation is shown in Equation (6).

$$\begin{cases} L_s \dfrac{di_s}{dt} = uv_{out} - v_s \\ C_{out} \dfrac{dv_{out}}{dt} = \dfrac{P_{const}}{v_{out}} - ui_s \end{cases} \tag{6}$$

where $u = d_{1\_buck}$ is the control signal. For the system in Equation (6), the set of the equilibrium point is ε_{x2} as shown in Equation (7).

$$\varepsilon_{x2} = \left\{ (i_s, v_{out}) \in \left(R^2_{>0} \middle| \frac{P_{const}}{v_{out}} - u i_s = 0 \right\} \right. \tag{7}$$

When the bi-dc converter operates in the buck state, the following *conclusion* could be obtained.

Corresponding to the output $y = i_s - i_{s*}$, the zero dynamics characteristic is stable, but it is not attractive at v_{out*}.

Proof: Based on the first equation in Equation (6), the control signal $u = v_s/v_{out}$ can be deduced when $i_s = i_{s*}$. Accordingly, Equation (8) can be derived by combining this result and the second equation in Equation (6).

$$\frac{dv_{out}}{dt} = \frac{1}{C_{out} v_{out}} (P_{const} - v_s i_{s*}) := f_2(v_{out}) \equiv 0 \tag{8}$$

Hence, it is proved that the system in Equation (6) at v_{out*} is stable, but it is not attractive at i_{s*}.

Remark 4: Although the bi-dc converter, when operating in buck state, does not show the non-minimum phase characteristics for i_s, PV and CPLs, existing as a current source, make the converter weak damping. The system is prone to oscillation. Besides, there is no zero dynamics for v_{out}.

Remark 5: The zero dynamics, corresponding to output i_s, is stable, but it is not attractive at v_{out*}. Therefore, when output voltage v_{out} is indirectly controlled through output current regulation, a steady-state voltage error would be caused depending on the initial condition.

3 | IDA-PBC CONTROL METHOD FOR BI-DC CONVERTER

First, the PCH modelling principle and process are briefly presented. Then, the IDA-PBC control law for bi-dc converter in different operation states is derived.

3.1 | IDA-PBC design

Normally, the PCH model of non-linear systems can be mathematically expressed as Equation (9).

$$\begin{cases} \dot{x} = [I(x) - D(x)] \cdot \frac{\partial E(x)}{\partial x} + \zeta + g(x) u \\ y = g^T(x) \frac{\partial E(x)}{\partial x} \end{cases} \tag{9}$$

where $I(x) = -I^T(x)$ and $D(x) = D^T(x)$ represent energy interchange and energy dissipation in the system, respectively, that is, the interconnection matrix and the dissipation matrix. $D(x)$ is a positive semidefinite matrix, that is, $D(x) \geq 0$. ζ represents the input signal, that is, the input voltage in this paper; u stands for the control signal, and y stands for the output quantity of the PCH model. The total energy function $E(x)$ is in Equations (10) and (11).

$$E(x) = \frac{1}{2L_s} x_1^2 + \frac{1}{2C_{out}} x_2^2 \tag{10}$$

$$x = (L_s i_s C_{out} v_{out})^T \tag{11}$$

As we all know, the system will stabilise at a certain equilibrium point eventually because of the dissipation property (represented by $D(x)$).

IDA-PBC method is adopted, making the non-linear system in Equation (9) take the PCH form in Equations (12) and (13) by modifying $I(x)$ and $D(x)$. $D_d(x) \geq 0$ is the desired damping matrix. A desired function $E_d(x)$ is established to replace energy function $E(x)$, and the control signal u is then derived. The internal energy interaction is completely changed and the dissipation property is assured. Hence, the non-linear system in Equation (9) can operate around the desired equilibrium x_* stably. Here, 'd' and 'a' imply desired and assigned matrices, respectively. The desired equilibrium point in a dc system can be the bus voltage reference value.

$$\dot{x} = [I_d(x) - D_d(x)] \cdot \frac{\partial E_d(x)}{\partial x} \tag{12}$$

$$\dot{x} = -[I_a(x) - D_a(x)] \cdot \frac{\partial E(x)}{\partial x} + \zeta \tag{13}$$

To obtain the desired energy function $E_d(x)$, an assigned energy function $E_a(x)$ is introduced. The relationship between $E_d(x)$ and $E_a(x)$ is shown in Equation (14). The requirements (Formulas 15–20) presented in Table 1 should also be satisfied.

$$E_a(x) = E_d(x) - E(x) \tag{14}$$

The system interconnection is modified by $I_a(x)$, and the system damping can be improved by $D_a(x)$, meaning that energy shaping and oscillation suppression can be achieved. It can be found from Equations (17) and (18) that the system can converge at the equilibrium point and asymptotic stability is assured.

TABLE 1 Requirements of interconnection and damping assignment passivity-based control

Structure preservation	$I_d(x) = I(x) + I_a(x) = -I_d^T(x)$ $D_d(x) = D(x) + D_a(x) = -D_d^T(x)$	Equation (15)
Integrability	$\frac{\partial^2 E_a(x)}{\partial x^2} = \left(\frac{\partial^2 E_a(x)}{\partial x^2}\right)^T$	Equation (16)
Equilibrium	$\frac{\partial E_d}{\partial x}(x_*) = 0$	Equation (17)
Lyapunov stability	$\frac{\partial^2 E_d}{\partial x^2}(x_*) > 0$	Equation (18)

3.2 | IDA-PBC control law of boost state

When the bi-dc converter is in the boost state and its output voltage is controlled, Equation (1) can be rewritten in PCH

form as shown in Equation (19).

$$\dot{x} = \begin{pmatrix} 0 & -\dfrac{1-d}{C_{\text{out}}} \\ \dfrac{1-d}{L_{\text{s}}} & -\dfrac{C_{\text{out}}P_{\text{const}}}{x_2^2} \end{pmatrix} \cdot x + \begin{pmatrix} 1 \\ 0 \end{pmatrix} V_{\text{s}} \tag{19}$$

Meanwhile, the interconnection and dissipation matrices ($I_{\text{boost}}(x)$ and $D_{\text{boost}}(x)$) are obtained ($u = 1–d$):

$$I_{\text{boost}}(x) = \begin{bmatrix} 0 & -(1-\text{d}) \\ (1-\text{d}) & 0 \end{bmatrix}, D_{\text{boost}}(x) = \begin{bmatrix} 0 & 0 \\ 0 & \dfrac{C_{\text{out}}P_{\text{const}}}{x_2^2} \end{bmatrix} \tag{20}$$

The expression of $E_{\text{d}}(x)$ is shown in Equation (21).

$$E_{\text{d}}(x) = \frac{1}{2L_{\text{s}}}(x_1 - x_{1*})^2 + \frac{1}{2C_{\text{out}}}(x_2 - x_{2*})^2 \tag{21}$$

$I_{\text{d\_boost}}(x)$ and $D_{\text{d\_boost}}(x)$ is defined as in Equation (22) and (23).

$$I_{\text{d\_boost}}(x) = 0 \tag{22}$$

$$D_{\text{d\_boost}}(x) = \begin{bmatrix} r_{1\_\text{boost}} & 0 \\ 0 & \dfrac{1}{r_{2\_\text{boost}}} + \dfrac{C_{\text{out}}^2 P_{\text{const}}}{x_2^2} \end{bmatrix} \tag{23}$$

According to Equation (15), the assigned interconnection and dissipation matrix can be obtained:

$$I_{\text{a\_boost}}(x) = \begin{bmatrix} 0 & (1-\text{d}) \\ -(1-\text{d}) & 0 \end{bmatrix},$$

$$D_{\text{a\_boost}}(x) = \begin{bmatrix} r_{1\_\text{boost}} & 0 \\ 0 & \dfrac{1}{r_{2\_\text{boost}}} \end{bmatrix} \tag{24}$$

Two different control laws can be obtained from Equations (1) and (12):

$$\begin{cases} d_{1\_\text{boost}} = 1 - \dfrac{V_{\text{s}} - r_{1\_\text{boost}}(i_{\text{s}} - i_{\text{s}*})}{v_{\text{out}}} \\ d_{2\_\text{boost}} = 1 - \dfrac{(v_{\text{out}} - v_{\text{out}*})}{r_{2\_\text{boost}} i_{\text{s}}} - \dfrac{i_{\text{out}} v_{\text{out}*}}{v_{\text{out}} i_{\text{s}}} \end{cases} \tag{25}$$

Theoretically, with proper injection damping (r_1 and/or r_2), d_{1_boost} and d_{2_boost} can achieve stable control of current and voltage, respectively. Practically, when the bi-dc converter operates as a boost circuit, it captures a non-minimum phase characteristic (*remark 1*). This puts a strict constraint on the controller bandwidth (*remark 3*) and reduces the dynamic response of the system. Without the rapid convergence of current, it is not possible to expect the voltage to quickly converge to the desired value (*remark 2*). Therefore, it is difficult to use d_{2_boost} to directly control voltage. In this paper, d_{1_boost} is adopted to form the IDA-PBC current loop.

3.3 | IDA-PBC control law of buck state

When operating in reverse, the bi-dc converter is a buck circuit, and the control goal is to stabilise its input voltage, and its differential equations in PCH form are obtained:

$$\dot{x} = \begin{pmatrix} 0 & \dfrac{d}{C_{\text{out}}} \\ -\dfrac{d}{L_{\text{s}}} & \dfrac{C_{\text{out}}P_{\text{const}}}{x_2^2} \end{pmatrix} \cdot x + \begin{pmatrix} -1 \\ 0 \end{pmatrix} V_{\text{s}} \tag{26}$$

$I_{\text{buck}}(x)$ and $D_{\text{buck}}(x)$ are obtained as shown in Equation (27). At this time, $D_{\text{buck}}(x)$ no longer reflects the dissipative characteristics, and its elements can be equivalent to negative resistance (a current source actually). This agrees with the analysis results of *remark 4*.

$$I_{\text{buck}}(x) = \begin{bmatrix} 0 & d \\ -d & 0 \end{bmatrix}, D_{\text{buck}}(x) = \begin{bmatrix} 0 & 0 \\ 0 & -\dfrac{C_{\text{out}}^2 P_{\text{const}}}{x_2^2} \end{bmatrix} \tag{27}$$

$I_{\text{d\_buck}}(x)$ and $D_{\text{d\_buck}}(x)$ is defined:

$$I_{\text{d\_buck}}(x) = 0, D_{\text{d\_buck}}(x) = \begin{bmatrix} r_{1\_\text{buck}} & 0 \\ 0 & \dfrac{1}{r_{2\_\text{buck}}} - \dfrac{C_{\text{out}}^2 P_{\text{const}}}{x_2^2} \end{bmatrix} \tag{28}$$

According to Equation (15), the assigned interconnection and dissipation matrix can be obtained:

$$I_{\text{a\_buck}}(x) = \begin{bmatrix} 0 & d \\ -d & 0 \end{bmatrix}, D_{\text{a\_buck}}(x) = \begin{bmatrix} r_{1\_\text{buck}} & 0 \\ 0 & \dfrac{1}{r_{2\_\text{buck}}} \end{bmatrix} \tag{29}$$

Two different control laws can be obtained from Equations (6) and (12):

$$\begin{cases} d_{1\_\text{buck}} = \dfrac{V_{\text{s}} - r_{1\_\text{buck}}(i_{\text{s}} - i_{\text{s}*})}{v_{\text{out}}} \\ d_{2\_\text{buck}} = \dfrac{(v_{\text{out}} - v_{\text{out}*})}{r_{2\_\text{buck}} i_{\text{s}}} + \dfrac{P_{\text{const}} v_{\text{out}*}}{v_{\text{out}}^2 i_{\text{s}}} \end{cases} \tag{30}$$

Practically, the rapid tracking of voltage reference requires the rapid change of battery current to complete energy balance. Therefore, in the absence of rapid current convergence, it is very difficult to expect the voltage to quickly converge to the desired value. Therefore, d_{1_boost} is adopted to form the IDA-PBC

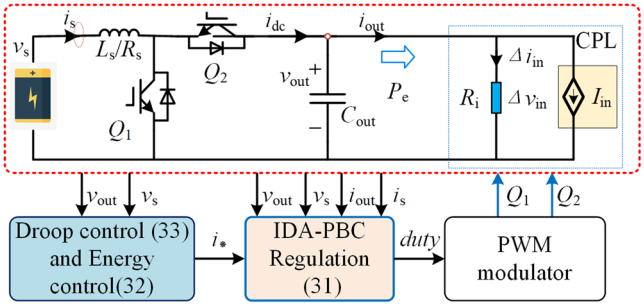

FIGURE 3 Control block diagram of the proposed interconnection and damping assignment passivity-based control (IDA-PBC) method

current inner loop.

$$\begin{cases} d_{1\_boost} = 1 - \dfrac{V_s - r_{1\_boost}\,(i_s - i_{s*})}{v_{out}}, Q_1 \\ d_{1\_buck} = \dfrac{V_s - r_{1\_buck}\,(i_s - i_{s*})}{v_{out}}, Q_2 \end{cases} \tag{31}$$

Considering the requirement of the boost state at the same time, it can be seen from Equations (25) and (30) that $d_{1\_buck} = 1 - d_{1\_boost}$ meets the requirement that the trigger pulse should be complementary. According to *remarks 2* and *4*, there would exist the steady-state output voltage error $\Delta v_{err}(\Delta v_{err} = v_{out*} - v_{out})$, if v_{out} is indirectly controlled by the current loop. An energy outer loop combined with adjustment factor k is introduced to eliminate Δv_{err}.

3.4 | IDA-PBC control law of boost state

Theoretically, the IDA-PBC controller can assure that v_{out} accurately tracks its reference value, if the system parameters and operation conditions are accurately available. However, in practice, because of the influences of zero dynamics and uncertainties of operation condition, Δv_{err} might occur in steady state, and the system might lose its stability when the load power changes suddenly (*remarks 2 and 5*).

$$\begin{cases} \dfrac{dS_e}{dt} = \dfrac{1}{2} k C_{out} \left(v_{out*}^2 - v_{out}^2\right) \\ i_{s*} = \dfrac{P_{const}}{V_s} = \dfrac{k_{pe} k C_{out} \left(v_{out*}^2 - v_{out}^2\right)/2 + k_{ie} S_e}{V_s} \end{cases} \tag{32}$$

In this paper, the objective of the introduced energy controller is to eliminate Δv_{err}. A PI controller $(k_{pe} + k_{ie}/s)$ is adopted to generate the power reference P_{ref}, using the error between output energy and its desired value. An adjustment factor k is introduced to adjust the transient response of the outer loop. Droop control (Equation 33) is utilised to realise multiple parallel operation. The control block diagram is in Figure 3.

$$v_{out*} = V_n - R_{droop} \cdot i_s \tag{33}$$

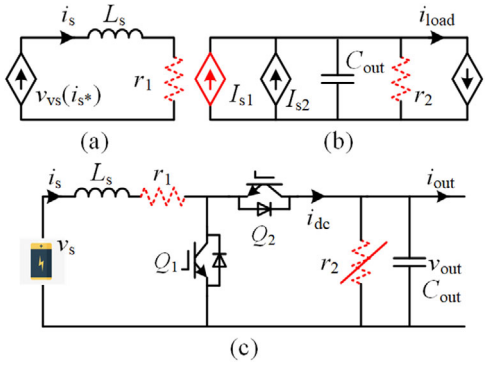

FIGURE 4 Equivalent circuit topology of bidirectional dc (bi-dc) converter under IDA-PBC. (a) Current formula, (b) voltage formula, and (c) bi-dc converter

4 | REPRESENTATION OF IDA-PBC

The introduction of $I_a(x)$ and $D_a(x)$ reshapes the energy interaction among different components and the energy dissipation property. The system passivity is assured. $D_a(x)$ can be equivalent to a virtual resistance, improving the system damping and smoothing the transient voltage. In this section, the virtual circuit is established to illustrate the physical meanings of IDA-PBC control parameters. The location of $D_a(x)$ is determined. The system dynamic characteristic is explained by Equations (12) and (13), which are rewritten as Equation (34). According to the physical meaning of each item, Equation (34) can be classified into real components (black colour) and virtual components (red colour) as shown in Figure 4.

$r_1 i_{s*}$ is regarded as a current-controlled voltage source $v_{vs}(i_{s*})$. The dissipation is modified by $D_a(x)$ representing the injected damping. Therefore, a virtual damping resistance r_1 is added as shown in Figure 4(a), which can tune the system damping. The voltage equations of the bi-dc converter in boost and buck state are shown in Equations (36b) and (36c), respectively. A virtual damping resistance r_2 is added as shown in Figure 4(b). In boost state, the term $v_{out*} P_{const}/v_{out}^2$ out is regarded as a voltage-controlled current source I_{s1}, providing power to the CPL and compensating for its negative incremental resistance influences. Because of $D_a(x)$, a virtual damping resistance r_2 is located at the output side, affecting the system damping. The term v_{out*}/r_2 is a constant current source I_{s2}, supplying power to linear loads. The difference between boost and buck state is that $v_{out*} P_{const}/v_{out}^2$ is a non-linear load in buck state to absorb the power from the equivalent source P_{const}/v_{out}. Based on the analysis mentioned above, the virtual circuit is constructed as shown in Figure 4(c).

$$L_s \frac{di_s}{dt} = i_{s*} r_1 - r_1 i_s \tag{34a}$$

$$C_{out} \frac{dv_{out}}{dt} = \frac{P_{const} v_{out*}}{v_{out}^2} - \frac{v_{out}}{r_2} - \frac{P_{const}}{v_{out}} + \frac{v_{out*}}{r_2} \tag{34b}$$

$$C_{out} \frac{dv_{out}}{dt} = \frac{P_{const}}{v_{out}} - \frac{v_{out}}{r_2} + \frac{v_{out*}}{r_2} - \frac{P_{const} v_{out*}}{v_{out}^2} \tag{34c}$$

Apparently, under the influence of virtual resistance, the energy interaction and dissipation are modified, and system damping becomes adjustable. Only r_1 is considered in this paper because of the zero dynamics analysis. The expression of the closed-loop system in boost and buck state, as shown in Equations (35a) and (35b), can be acquired by combining Equations (31) with (19) and (26), respectively.

$$\dot{x} = \begin{pmatrix} -\frac{r_1}{L_s} & -\frac{1-d}{C_{out}} \\ \frac{1-d}{L_s} & -\frac{C_{out}P_{const}}{x_2^2} \end{pmatrix} \cdot x + \begin{pmatrix} 1 \\ 0 \end{pmatrix} V_s \tag{35a}$$

$$\dot{x} = \begin{pmatrix} -\frac{r_1}{L_s} & \frac{d}{C_{out}} \\ -\frac{d}{L_s} & \frac{C_{out}P_{const}}{x_2^2} \end{pmatrix} \cdot x + \begin{pmatrix} -1 \\ 0 \end{pmatrix} V_s \tag{35b}$$

$$G_{boost}(s) = \frac{\Delta i_s}{\Delta d} = \frac{\frac{(1-D)I_s}{L_sC_{out}} + \left(\frac{sC_{out}}{L_sC_{out}} - \frac{P_{const}}{L_sC_{out}v_{out}^2}\right)}{s^2 + s\left(\frac{r_1}{L_s} - \frac{P_{const}}{C_{out}v_{out*}^2}\right) - \frac{r_1}{L_sC_{out}}\frac{P_{const}}{v_{out*}^2} + \frac{(1-D)^2}{L_sC_{out}}} \tag{36a}$$

$$G_{buck}(s) = \frac{\Delta i_s}{\Delta d} = \frac{\frac{(v_{out*}-I_sD)}{L_sC_{out}}}{s^2 + s\left(\frac{r_1}{L_s} + \frac{P_{const}}{C_{out}v_{out*}^2}\right) + \frac{r_1}{L_sC_{out}}\frac{P_{const}}{v_{out*}^2} + \frac{D^2}{L_sC_{out}}} \tag{36b}$$

Linearizing Equation (35) around x_*, the transfer function between Δi_s and Δd can be obtained as shown in Equation (36).

5 | DYNAMICS ANALYSIS AND PASSIVITY VERIFICATION

When the bi-dc converter is running in the boost state, CPL reduces the system damping and the system is prone to oscillation. Besides, the current inner loop has an RHP zero affected by the operation point (*remarks 1* and *3*), which negatively affects the control performance. Therefore, the dynamic characteristics in the boost state will be analysed emphatically.

5.1 | Inner-loop dynamics analysis and its parameters design

From Equation (36a), the calculation formulas for damping ratio ξ, natural oscillation frequency ω_n and overshoot σ can be obtained as shown in Equation (37). The influence of r_1 on damping ratio ξ and overshoot σ is shown in Figure 5(a). With r_1 increasing, ξ increases gradually and the overshoot σ decreases. Particularly when $\xi = 1$, there is no overshoot during the dynamic and the critical value of r_1 can be calculated by Equation (38). To meet the stability requirement, the real part of the eigenvalues of the closed-loop system must be negative. Hence, the lower bound of r_1 can be obtained as shown in Equation (39).

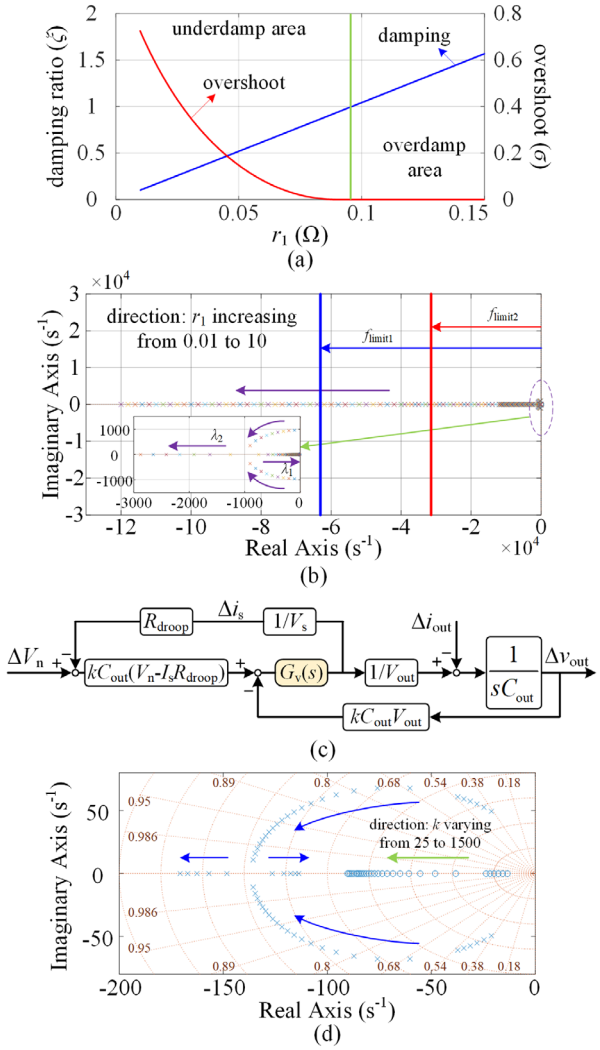

FIGURE 5 Dynamics analysis and parameters design. (a) Effect of r_1 on ξ and overshoot σ, (b) eigenvalues varying with different r_1, (c) small-signal model of the outer loop, and (d) the zero and pole distribution of the $T_{vo}(s)$ when k varies

$$\xi = \frac{\frac{r_1}{L_s} - \frac{1}{C_{out}}\frac{P_{const}}{v_{out}^2}}{2\sqrt{\frac{(1-D)^2}{L_sC_{out}} + \frac{r_1}{L_sC_{out}}\frac{P_{const}}{v_{out}^2}}} \tag{37a}$$

$$\omega_n = \sqrt{\frac{(1-D)^2}{L_sC_{out}} - \frac{r_1}{L_sC_{out}}\frac{P_{const}}{v_{out*}^2}} \tag{37b}$$

$$\sigma\% = \exp\left(-\frac{\pi\xi}{\sqrt{1-\xi^2}}\right) \times 100\% \tag{37c}$$

$$r_{1\_critical} = 2\sqrt{\frac{L_s}{C_{out}}(1-D)} - \frac{L_s}{C_{out}}\frac{P_{const}}{v_{out}^2} \tag{38}$$

$$\text{real}\left(\lambda_{1,2}\right) = -\omega_n\xi < 0, \rightarrow r_1 > \frac{L_s P_{const}}{C_{out} v_{out}^2} \tag{39}$$

With the injected damping increasing, the energy dissipation of the bi-dc converter would be theoretically enhanced, but the transient time of the inner loop would be prolonged also. The coordination between the inner and outer loop would become difficult when the inner loop is slow, which is not conducive to the stable control of the system. Therefore, the value of r_1 needs to be limited. Meanwhile, the factors affecting the system dynamics, such as switching frequency f_s, output capacitance and load, should be considered, when the value for r_1 is selected.

The effectiveness of the inner-loop transfer function can be only assured within the frequency range where the bi-dc converter works. Within this frequency range, the average value of voltage and current can be calculated and the state-space average model is valid. Therefore, the location of the dominant poles is subjected to the effectiveness of the system averaged model. Hence, the upper limit of r_1 can be determined.

Generally, the behaviour of the converter is analysed well below the Nyquist frequency (i.e. $0.5f_s$). To make the state-space average model more accurate, stricter restrictions can be imposed on the frequency band under study, such as $0.1f_s$.

The eigenvalues (λ_1, λ_2) distribution is shown in Figure 5(b). To meet different requirements, two frequency limits are set, $f_{limit1} = f_s = 10$ kHz and $f_{limit2} = 0.5f_s = 5$ kHz. According to the dynamic response requirements, the appropriate r_1 can be selected within different limits. The concept of the dominant pole is used to approximate the system. The current loop under the IDA-PBC law is equivalent to a first-order inertia loop due to its small time constant. The closed-loop transfer function is

$$G_{i\_clo}(s) = \frac{1}{sT+1}, T \approx \frac{1}{\min \text{real}\left(-\lambda_1, -\lambda_2\right)} \tag{40}$$

5.2 | Outer-loop dynamics analysis and its parameters design

Linearising Equation (32) and integrating its result and Figure 3, the small-signal model of energy loop is established and shown in Figure 5(c). Because of the fast response, the inner loop is equivalent to a unity gain block. The relationship between Δv_{out} and its reference is obtained as shown in Equation (41).

$$T_{vo} = \frac{\Delta v_{out}}{\Delta V_n} = \frac{1+\tau_1 s}{\left(\frac{s}{\omega_{n1}}\right)^2 + \frac{2\xi_1}{\omega_{n1}}s + 1} \tag{41}$$

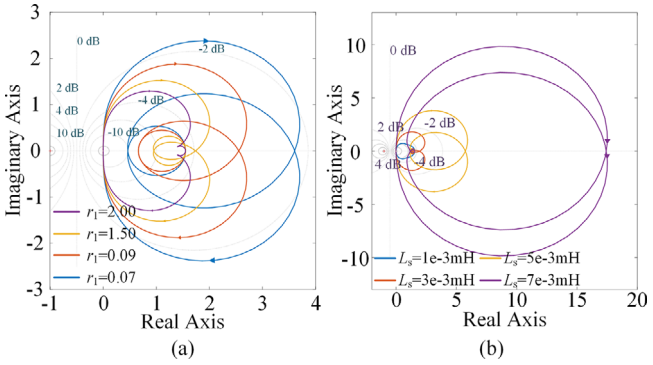

FIGURE 6 Nyquist plot of output impedance. (a) Output impedance when r_1 changes, (b) output impedance when L_s changes

where

$$\tau_1 = k_{pe}/k_{ie}, \omega_{n1} = \sqrt{\frac{k_{ie}V_s}{V_s/k + C_{out}V_{out}R_{droop}}} \tag{42a}$$

$$\xi_1 = \frac{\left(C_{out}V_{out}R_{droop}k_{ie} + V_s k_{pe}\right)}{2\sqrt{\left(V_s/k + C_{out}V_{out}R_{droop}\right)k_{ie}V_s}} \tag{42b}$$

Considering practice applications, the transient response would be prolonged, when k selects a large value. According to Equations (41) and (42), the zeros and poles distribution is shown in Figure 5(d), when k changes from 25 to 1500. A pair of conjugate poles near the imaginary axis gradually moves away from the point (0, 0), meaning the damping improvement is achieved. As k increases, the conjugate poles become a pair of negative real poles. One of the negative real poles moves toward the imaginary axis and it should not move into the RHP, meaning the system is always stable.

5.3 | Passivity analysis

In this part, we perform passivity analysis supporting the previous performance analysis, which is based on the equivalent circuit. The Nyquist plot of output impedance is illustrated in Figure 6. With r_1 varying in a reasonable range, most of the Nyquist plots are in the RHP, meaning that the bi-dc converter system could maintain passive and stable. It can be observed from Figure 6(a) that the passivity is enhanced gradually while r_1 increases in a reasonable range. In Figure 6(b), a variation of filter inductances L_s was performed. Increasing L_s can reduce the harmonic content of the current. However, the passivity is weakened and the stability margin is also reduced. The entire system always remains passive. Therefore, the appropriate inductance value should be selected, considering its influence on the system stability and the filtering effect at the same time. Besides, Figure 6(b) highlights the application advantages of the IDA-PBC method. If those passive components (or systems) are connected in parallel, the resulting system will still be passive.

TABLE 2 The parameters of the simulation

Subsystem	Parameters	Magnitude
Bidirectional dc converter	Input voltage (v_s)	100 V
	Input filter inductor (L_s/R_s)	5 mH/0.01 Ω
	Capacitance (C_{out})	2000 μF
	Switching frequency	10 kHz
Buck converter	Load voltage (v_{out_buck})	100 V
	Load power (P_{const} (R))	2000 W (5Ω)
	Input capacitance (C_{in})	1200 μF
	Filter inductor (L_f/R_f)	4 mH/0.01 Ω
	Output capacitance (C_f)	1000 μF
DC bus	DC bus voltage (v_{dc_bus})	300 V
	DC bus capacitance (C_{bus})	3000 μF
	Line impedance (R_{line}/L_{line})	0.01 Ω/0.1 mH
Control parameter	Energy controller	$k_{pe} = 2$, $k_{ie} = 200$
	r_1	0.05
	k	250

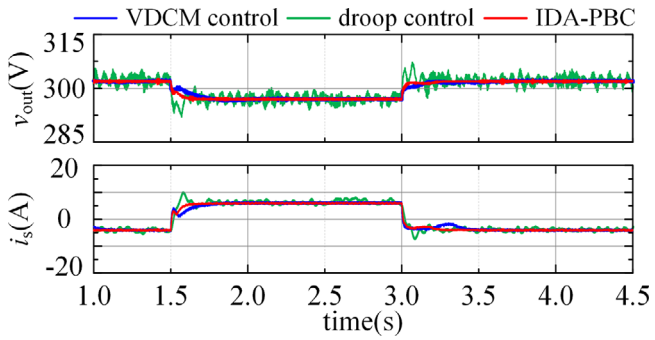

FIGURE 7 The simulation results of different control strategies

6 | SIMULATION VERIFICATION

To test the proposed control strategy, an isolated dc distribution system similar to that in Figure 1 is modelled in MATLAB. Loads are replaced by CPLs. The parameters of the simulation are in Table 2. The load suddenly increases by 1kW at $t = 1.5$ s and decreases by 1kW at $t = 3.0$ s.

6.1 | Comparison among different control strategies

Figure 7 depicts the simulation results under conventional droop control, virtual inertia control (VIC) and the proposed IDA-PBC, respectively. When the load changes suddenly, v_{out} under the traditional droop control is more prone to oscillation. This indicates that the system is inertialess and weak damping. While VIC is adopted and appropriate control parameters are selected, v_{out} would smoothly transition to another steady state. This phenomenon indicates the VIC can improve the system inertia. And the IDA-PBC, with less parameter to select, can achieve the same control effect as VIC. Hence, the system damping is effectively enhanced by the proposed IDA-PBC method.

6.2 | Influences of control parameters on the transient response

Figures 8(a) and (b) show the impact of r_1 and k on the dynamic response when the system is disturbed. With r_1 or k increasing, the dc bus voltage oscillation has been significantly suppressed. The energy dissipation property and the damping performance is enhanced obviously, making the system stable even if a disturbance occurs. It can be observed that control parameters vary with a large interval. The converter system is a strongly nonlinear system. Therefore, there are the case where the control parameters need to be changed within a large range to obtain different control effects and the case where control effects change greatly when the control parameters change with a small interval.

Figures 8(c) and (d) display the necessity of setting an upper limit for r_1. When r_1 chooses a little value, the harmonic content is low and total harmonic distortion (THD) is about 1.64%. The harmonic content rises apparently with a large r_1, and THD is about 16.72%. Therefore, when r_1 is determined, the trade-off between the system damping and harmonic content should be considered.

7 | CONCLUSION

An IDA-PBC method, guided by zero dynamics analysis, is proposed to improve the transient response of dc distribution system. The control law derivation, implementation, dynamic analysis, parameters design and passivity verification are studied in detail. Simulation demonstrates its validity. The main conclusions are:

1. The RHP zero will reduce the stability margin of the bi-dc converter and impose a constraint on the controller design. A steady-state error will be caused.
2. An IDA-PBC method is achieved via modifying the energy interaction and dissipation. It has better performance and comparatively less tuning parameters. The steady-state error can be eliminated by an energy controller.
3. A virtual circuit that explains the physical significance of the control parameter is established. The reasonable range of the control parameters is obtained by the dynamic response. Larger r_1 will increase the harmonic content and larger k would prolong the transient response, destructing the stable operation.
4. Impedance-based passivity analysis verifies the performance of the proposed IDA-PBC method, which has the same control effect as the VIC.

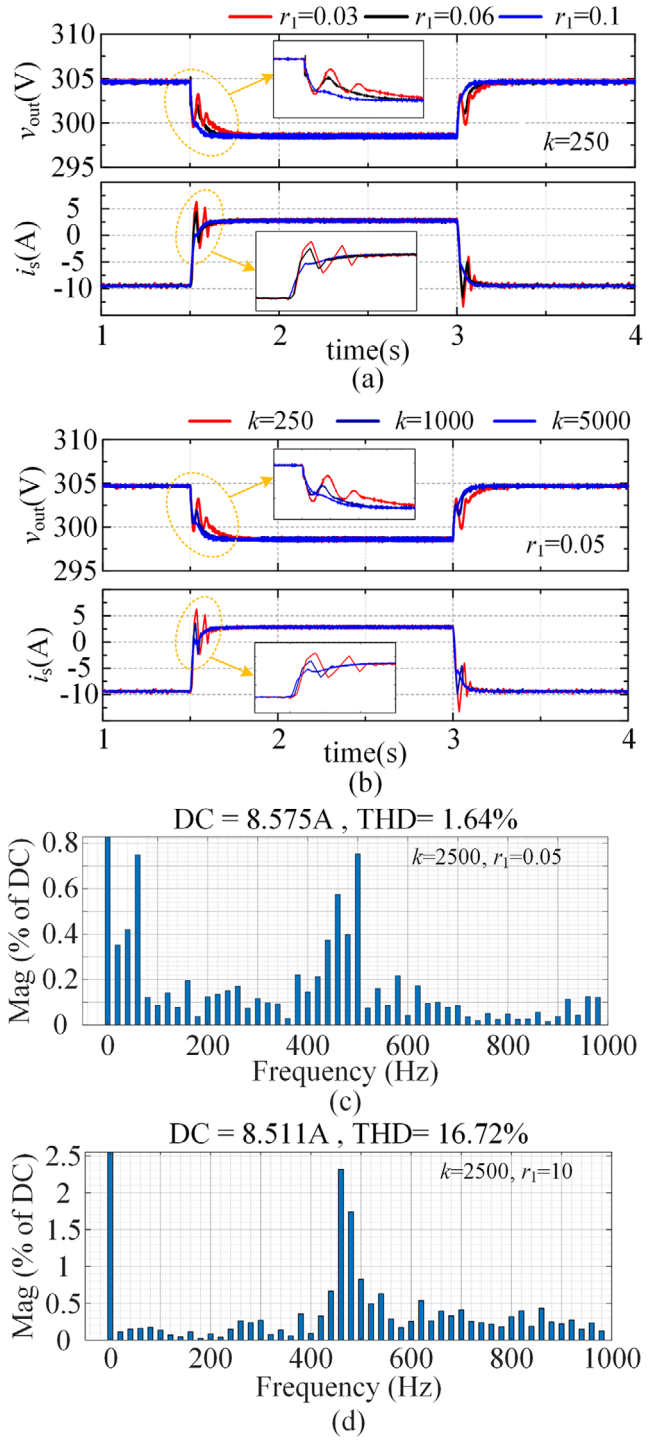

FIGURE 8 Simulation results and harmonic content analysis. (a) Different values of r_1, (b) different values of k, (c) the influence of r_1 on harmonic content ($r_1 = 0.05$), and (d) the influence of r_1 on harmonic content ($r_1 = 10$)

Future work will focus on the adaptive adjustment of control parameters.

ACKNOWLEDGEMENT

This work is supported in part by China Scholarship Council (No. 201906130196).

Open access funding enabled and organized by Projekt DEAL.

ORCID

Gang Lin https://orcid.org/0000-0002-5214-6891

REFERENCES

1. Madduri, P.A., et al.: Scalable DC microgrids for rural electrification in emerging regions. IEEE J. Emerging Sel. Top. Power Electron. 4(4), 1195–1205 (2016)
2. Perez, F., et al.: Stability analysis of a DC MicroGrid for a smart railway station integrating renewable sources. IEEE Trans. Control Syst. Technol. 28, 1802–1816 (2019)
3. Gao, F., et al.: Control design and voltage stability analysis of a droop-controlled electrical power system for more electric aircraft. IEEE Trans. Ind. Electron. 64(12), 9271–9281 (2017)
4. Tabari, M., Yazdani, A.: Stability of a dc distribution system for power system integration of plug-in hybrid electric vehicles. IEEE Trans. Smart Grid 5(5), 2564–2573 (2014)
5. Karbalaye Zadeh, M., et al.: Stability analysis and dynamic performance evaluation of a power electronics-based DC distribution system with active stabilizer. IEEE J. Emerging Sel. Top. Power Electron. 4(1), 93–102 (2016)
6. Cespedes, M., Xing, L., Sun, J.: Constant-power load system stabilization by passive damping. IEEE Trans. Power Electron. 26(7), 1832–1836 (2011)
7. Guo, L., et al.: Stability analysis and damping enhancement based on frequency-dependent virtual impedance for DC microgrids. IEEE J. Emerging Sel. Top. Power Electron. 5(1), 338–350 (2017)
8. Song, X., et al.: Active damping stabilization for high-speed BLDCM drive system based on band-pass filter. IEEE Trans. Power Electron. 32(7), 5438–5449 (2017)
9. Zhang, X., Ruan, X., Zhong, Q.: Improving the stability of cascaded DC/DC converter systems via shaping the input impedance of the load converter with a parallel or series virtual impedance. IEEE Trans. Ind. Electron. 62(12), 7499–7512 (2015)
10. Wu, M., Lu, D.D.: A novel stabilization method of LC input filter with constant power loads without load performance compromise in DC microgrids. IEEE Trans. Ind. Electron. 62(7), 4552–4562 (2015)
11. Zhu, X., et al.: An inertia and damping control method of DC–DC converter in DC microgrids. IEEE Trans. Energy Convers. 35(2), 799–807 (2020)
12. Siegers, J., Arrua, S., Santi, E.: Stabilizing controller design for multibus MVdc distribution systems using a passivity-based stability criterion and positive feedforward control. IEEE J. Emerging Sel. Top. Power Electron. 5(1), 14–27 (2017)
13. del Puerto-Flores, D., et al.: Passivity-based control by series/parallel damping of single-phase PWM voltage source converter. IEEE Trans. Control Syst. Technol. 22(4), 1310–1322 (2014)
14. Son, Y.I., Kim, I.H.: Complementary PID controller to passivity-based nonlinear control of boost converters with inductor resistance. IEEE Trans. Control Syst. Technol. 20(3), 826–834 (2012)
15. Hassan, M.A., et al.: Adaptive passivity-based control of dc-dc buck power converter with constant power load in dc microgrid systems. IEEE J. Emerging Sel. Top. Power Electron. 7(3), 2029–2040 (2019)
16. Ortega, R., et al.: Interconnection and damping assignment passivity-based control of port-controlled Hamiltonian systems. Automatica 38(4), 585–596 (2002)
17. Ortega, R., Garcia-Canseco, E.: Interconnection and damping assignment passivity-based control: A survey. Eur. J. Control 10(5), 432–450 (2004)
18. Samanta, S., et al.: Design of an interconnection and damping assignment-passivity based control technique for energy management and damping improvement of a DC microgrid. IET Gener. Transm. Distrib. 14(11), 2082–2091 (2020)
19. Meshram, R.V., et al.: Port-controlled phasor hamiltonian modeling and IDA-PBC control of solid-state transformer. IEEE Trans. Control Syst. Technol. 27(1), 161–174 (2019)

20. He, W., et al.: An adaptive passivity-based controller of a Buck-Boost converter with a constant power load. Asian J. Control 21(1), 581–595 (2019)
21. Pang, S., et al.: Interconnection and damping assignment passivity-based control applied to on-board DC–DC power converter system supplying constant power load. IEEE Trans. Ind. Appl. 55(6), 6476–6485 (2019)
22. Pang, S., et al.: Improving the stability of cascaded DC-DC converter systems via the viewpoints of passivity-based control and port-controlled Hamiltonian framework. In: 2019 IEEE Industry Applications Society Annual Meeting, Baltimore, MD, USA, pp. 1–6 (2019)
23. Zeng, J., Zhang, Z., Qiao, W.: An interconnection and damping assignment passivity-based controller for a DC-DC boost converter with a constant power load. IEEE Trans. Ind. Appl. 50(4), 2314–2322 (2014)
24. Pang, S., et al.: Towards stabilization of constant power loads using IDA-PBC for cascaded LC filter DC/DC converters. IEEE J. Emerging Sel. Top. Power Electron. 1-1 (2019). https://doi.org/10.1109/JESTPE.2019.2945331
25. Pang, S., et al.: Large-signal stable nonlinear control of DC/DC power converter with online estimation of uncertainties. IEEE J. Emerging Sel. Top. Power Electron. 1-1 (2020). https://doi.org/10.1109/JESTPE.2020.3010895
26. Pang, S., et al.: Large-signal stabilization of power converters cascaded input filter using adaptive energy shaping control. IEEE Trans. Transp. Electrif. 1-1 (2020). https://doi.org/10.1109/TTE.2020.3021954
27. Cupelli, M., et al.: Port controlled hamiltonian modeling and IDA-PBC control of dual active bridge converters for DC microgrids. IEEE Trans. Ind. Electron. 66(11), 9065–9075 (2019)
28. Kwasinski, A., Krein, P.T.: Passivity-based control of buck converters with constant-power loads. In: 2007 IEEE Power Electronics Specialists Conference, Orlando, FL, pp. 259–265 (2007)

How to cite this article: Lin G, Liu J, Rehtanz C, Li Y, Zuo W, Wang P. Analysis of instability causes in the bi-dc converter and enhancing its performance by improving the damping in the IDA-PBC control. IET Gener Transm Distrib. 2021;15:2411–2421. https://doi.org/10.1049/gtd2.12169